Calculated magneto-optical properties of cubic and tetragonal Fe, Co, and Ni

Anna Delin, Olle Eriksson, and Börje Johansson
Condensed Matter Theory Group, Department of Physics, Uppsala University, P.O. Box 530, S-75121 Uppsala, Sweden

Sushil Auluck
Department of Physics, Roorkee University, Roorkee 247 667, India

J. M. Wills
Theoretical Division, Los Alamos National Laboratory, Los Alamos, New Mexico 87544
(Received 21 May 1999)

Recent experiments suggest that the linear magneto-optical signal from thin surfaces differs significantly from the corresponding bulk signal. Using an *ab initio* full potential linear muffin-tin orbital method, we have therefore calculated the polar magneto-optical Kerr signal for tetragonal and cubic Fe, Co, and Ni, in order to elucidate the role of tetragonal distortion on magneto-optical spectra. Our calculations indicate that for all three metals, the amplitudes and positions of the peaks in the Kerr spectra do change due to the tetragonal distortion, but the effect is not dramatic, and far from the observed differences. We therefore conclude that the large observed differences must have another origin, and discuss possible sources. Furthermore, since magneto-optical spectra are very sensitive to details in the wave functions and density, calculation of such spectra constitutes an important test of any *ab initio* method. The highly accurate method used in the present calculations differs from previously used methods in several respects, and a comparison between the different methods is made. [S0163-1829(99)04340-4]

I. INTRODUCTION

Plane-polarized light reflected from a magnetized material becomes elliptically polarized, and the plane of polarization is rotated. This effect is called the magneto-optical Kerr effect (MOKE), after its discoverer. Typically, the effect is not very large. Reflection against the ferromagnetic $3d$ transition metals Fe, Co, and Ni causes rotations smaller than $1°$. In more exotic materials, such as half-metals and materials containing f elements, the Kerr rotation may be much larger. The most extreme example is CeSb, where the Kerr rotation reaches its maximum possible value, $90°$.[1] The nonlinear Kerr effect combines frequency multiplication with the mentioned changes of the polarization. In general, the nonlinear Kerr signals are much more dramatic than the linear correspondents.[2] In the present study, the Kerr effect is understood to mean the linear Kerr effect only. We also limit ourselves to the polar geometry, i.e., the spin and photon directions are both assumed to be perpendicular to the surface. Experimentally, this is the most studied geometry, and is also the one which in general gives the largest Kerr signal.

The microscopic origin of the Kerr effect is a combined action of spin-orbit coupling and the net spin-polarization of the material.[3] The effect is sensitive to small changes in the band structure and eigenfunctions, and a more accurate treatment of the electronic structure, e.g., by using a full-potential treatment and a basis set which can systematically be enlarged without becoming overcomplete, should therefore result in visible changes in the spectra. This also means that calculation of such spectra constitutes an important test of any calculational method, which in itself is an important motivation for the present work.

To first order, the changes in polarization and ellipticity are proportional to the sample magnetization, and the Kerr effect is therefore useful experimentally in measurements of the magnetic moment. In recent times, it has rapidly developed into a widely used probe in many research fields, such as, e.g., surface magnetism,[4] magnetic interlayer coupling in multilayers,[5] and structural and magnetic anisotropies.[6] A well-known technological application is in the read-out process in high-density digital information storage systems.[7] For a general review of the present status of experimental and theoretical magneto-optic research, see, e.g., Refs. 8–12.

Low-dimensional magnetic structures such as surfaces and thin films have become a new and exciting field of research and applications. They exhibit many exotic phenomena, which are absent in bulk systems. However, also the pure bulk properties of the constituents used in these systems may be changed. For example, as soon as a thin film of one material is applied on some substrate, whose lattice parameter does not exactly match the lattice parameter of the film, a distortion of the crystal structure of the film occurs. Very recently, Nakajima *et al.*[13] presented results indicating that the optical conductivities from tetragonally distorted Ni and Co films are significantly different from those derived from measurements on the corresponding cubic materials. The differences are of two types. First, the amplitudes of the conductivities change rather drastically. Second, the peak positions are altered. The effects are especially predominant in the off-diagonal conductivity. It is, of course, of high interest to investigate whether these differences are mostly due to the tetragonal distortion of the interior of the film, or if surface and substrate effects or differences in the experimental approach play important roles in creating these differences. In the present study, our primary goal is to investigate how the Kerr signal is affected by tetragonal distortion. For this pur-

pose, we have calculated the Kerr spectra for cubic and tetragonal Fe, Co, and Ni. The in-plane lattice parameter of Co and Ni was taken to be that of Cu (fcc), and for Fe, it was taken to be that of V (bcc). Fe films grown on Cu are not necessarily ferromagnetic, and, furthermore, the tetragonal distortion of Fe grown on Cu is extremely small. For these reasons, we have chosen to omit that system in the present calculations.

Experimentally, Co on Cu (001) is one of the best examples of a tetragonally stabilized system. After the first couple of monolayers, Co on Cu (001) grows tetragonally with good structural order up to 50 to 70 monolayers. As the film grows thicker, the lattice parameter will relax toward its bulk value. For both Co and Ni, grown on a Cu substrate, the bulk lattice parameter is achieved after about 200 monolayers.[13] A Co film exhibiting fcc structure was first reported by Suzuki *et al.*[14] They measured the atomic volume in their fcc Co films to be the same as for bulk hcp Co.

The magneto-optical properties of Co and Ni grown on Cu have been investigated in some detail.[13] Spectra were registered for two different thicknesses, 20 Å and 1000 Å. In the thinner films, the in-plane lattice parameter is close to that of Cu, but already at about 200 Å, the in-plane lattice parameter has relaxed to the bulk value.

Fe on V is a much less stable system than the above-mentioned one. Growing Fe on V will cause the in-plane lattice parameter to expand around 5%, which is a rather large expansion. Fe will therefore grow epitaxially only the first couple of monolayers, after which dislocations set in.

A large number of measurements of the magneto-optical properties of bulk Fe, Co, and Ni have been performed. Erskine and Stern[15] studied the off-diagonal optical conductivity of all three metals using ellipsometric techniques and the longitudinal Kerr geometry. Later, these measurements for Ni were extended beyond the quartz limit by Erskine.[16] Krinchik and Artemjev[17] measured magneto-optical spectra of all three metals, both in the polar and equatorial Kerr geometries. Višňovský *et al.*[18] compared bulk Fe polar Kerr spectra with Fe films built on various substrates. Weller *et al.*[19] investigated the orientation dependence of the polar Kerr effect in both fcc and hcp Co. The polar Kerr effect for Ni at low temperature was investigated experimentally by Di and Uchiyama.[20] Interestingly, the low-temperature spectrum differs substantially from room-temperature data.

The diagonal optical constants of Fe, Co, and Ni have been measured and analyzed by a large number of authors, and we can only mention a few of them here. Johnson and Christy[21] measured and compared the diagonal optical constants for several transition metals, including the three we treat here. Shiga and Pells[22] performed measurements, with Drude's method, of the diagonal optical conductivity of Ni, as a function of temperature, and made a careful analysis of the origins of the peaks in the spectra, with respect to band structure. Bolotin, Kirillova, and Mayevskiy[23] measured the diagonal optical conductivity of Fe and discussed the relation between the spectrum and the Fermi surface. The diagonal optical constants of Fe were also determined by Yolken and Kruger,[24] using ellipsometry. They emphasize the influence of surface preparation on the measured optical constants. Recently, Fu *et al.*[25] measured the diagonal dielectric function of fcc Co. Ehrenreich, Philipp, and Olechna[26] obtained the diagonal dielectric constant for Ni from reflectance measurements and interpreted the structures in the spectrum in terms of interband transitions between the Fermi surface and the $3d$ band.

Many of the experimental spectra differ substantially from each other. Reasons for this are, e.g., differences in sample quality, method of annealing, surface polishing, and the degree of magnetization. Also, differences in the experimental technique and different extrapolation procedures used in the calculation of the conductivity from measured spectra may contribute to these differences.

The absorptive off-diagonal optical conductivities for Fe, Co, and Ni have been calculated previously, using modern band-structure methods, see, e.g., Refs. 27–29.

Calculated polar Kerr spectra of cubic Fe, Co, and Ni have been published by several authors. Oppeneer *et al.*[30] calculated the MOKE of cubic Fe, Co, and Ni using a linear muffin-tin orbital (LMTO) method in the atomic spheres approximation (ASA), including combined corrections. In their method, both parts of the complex optical conductivity are calculated directly using the Kubo formula[32,33] with finite relaxation time. Guo and Ebert[34] calculated the orientation dependence of the MOKE in fcc Co, using the spin-polarized, relativistic linear muffin-tin orbital (SPRLTMO) method in the ASA, without combined corrections.

Gasche, Brooks, and Johansson[35] investigated the effect of orbital polarization on the MOKE spectra of Fe, Co, and Ni. Their calculational method is similar to the one used by Oppeneer *et al.*, but they also compared the finite-relaxation-time approach via an alternative path, namely to calculate only the absorptive part in the limit of sharp band states (infinite lifetime) and then perform the Kramers-Kronig transformation to obtain the dispersive part. Mainkar, Browne, and Callaway calculated the MOKE and also the equatorial Kerr effect using a LCGO method.[36] Maclaren and Huang calculated the polar Kerr effect in Fe and Co, using the full-potential linear augmented Slater orbital (FLASTO) method, however without including any f states in the basis.[37] Our calculational method differs from most of the previously used methods in that it is a full-potential method, i.e., no shape approximation of the potential, wave functions, or density has been employed, combined with a very flexible basis set which can be systematically improved upon without becoming overcomplete, which may be a problem in methods where the basis set is constructed from Gaussian or Slater orbitals. Especially for metallic systems, such a flexible basis set should be important. Furthermore, no calculation of the optical spectra of tetragonally distorted Fe, Co, and Ni has previously been reported.

II. MACROSCOPIC THEORY OF MAGNETO-OPTICS

At optical frequencies the propagation of electromagnetic waves in magnetic materials may be fully described by the dielectric tensor $\boldsymbol{\epsilon}$, or equivalently, with the optical conductivity tensor $\boldsymbol{\sigma}$.[38] For the materials studied here, the optical conductivity is a symmetric tensor in the absence of a magnetic field. For cubic crystals, in the absence of an external or internal magnetic field, the optical conductivity tensor is diagonal in the crystal axes, with all three diagonal elements equal. In this case, the tensor will have the same properties

as a scalar. Applying a magnetic field will break time-reversal symmetry since the magnetic field changes sign under time reversal, causing magneto-optical effects to appear. When time-reversal symmetry is broken, the system reacts differently to photons with helicity 1 (spin and momentum parallel), compared to photons with helicity -1 (spin and momentum antiparallel), which is the time-reversed correspondent. In this case, the optical conductivity tensor is no longer symmetric, and it can be written as the sum of a Hermitian part, containing the dispersive components, and an anti-Hermitian part, containing the absorptive components. Thus, with the magnetic moment in the z direction, the form of the optical conductivity tensor in the present case is

$$\boldsymbol{\sigma}=\boldsymbol{\sigma}^{(1)}+i\boldsymbol{\sigma}^{(2)}=\begin{pmatrix}\sigma_{xx} & \sigma_{xy} & 0\\ \sigma_{yx} & \sigma_{yy} & 0\\ 0 & 0 & \sigma_{zz}\end{pmatrix}, \tag{1}$$

where $\sigma_{xx}=\sigma_{yy}$ and $\sigma_{yx}=-\sigma_{xy}$. Note that even in the cubic case, σ_{zz} is not strictly equal to σ_{xx}. The difference, however, is very small for the materials studied here, at least in the cubic structures.[39]

In standard notation, the real component of diagonal elements describes the ordinary optical absorption which is always positive, and the imaginary component of off-diagonal elements describes the magneto-optical absorption. The absorptive part of the off-diagonal optical conductivity has a direct physical interpretation. It is proportional to the difference in absorption of left and right circularly polarized light, and its sign is directly related to the spin polarization of the states responsible for the interband transitions producing structure in the spectra.

As mentioned, MOKE refers to the change in the polarization of light reflected from the surface of a magnetic material. Linearly polarized light is turned into elliptically polarized light with ellipticity ϵ_K and its major axis is rotated by the Kerr rotation angle θ_K relative to the polarization axis of the incident beam. Both quantities, which are usually combined into the complex Kerr angle $\theta_K+i\epsilon_K$, can be related to the optical conductivity of the material. For the polar geometry, the Kerr rotation and ellipticity can be calculated from the implicit expression[12]

$$\frac{1+\tan\epsilon_K}{1-\tan\epsilon_K}e^{2i\theta_K}=\frac{(1+n_+)}{(1-n_+)}\frac{(1-n_-)}{(1+n_-)}, \tag{2}$$

where $n_\pm^2$ are eigenvalues of the dielectric function tensor corresponding to Eq. (1), explicitly,

$$n_\pm^2=1+\frac{4\pi i}{\omega}(\sigma_{xx}\pm i\sigma_{xy}). \tag{3}$$

For small Kerr angles, this can be simplified to[40]

$$\theta_K+i\epsilon_K=\frac{-\sigma_{xy}}{\sigma_{xx}\sqrt{1+\frac{4\pi i}{\omega}\sigma_{xx}}}. \tag{4}$$

Note that the roots of the real and imaginary parts of σ_{xy} in general do not coincide with zero amplitude of the Kerr signals θ_K and/or ϵ_K.

III. DETAILS OF THE CALCULATIONS

A. General considerations

Throughout our calculations, we have assumed a polar geometry, i.e., the direction of light propagation is perpendicular to the surface and the spin moment is parallel to the outgoing light. Furthermore, the calculations are relativistic and spin-polarized, as they must be, in order to obtain a magneto-optical signal.

All calculations presented here are bulk calculations. The main reason is that we wish to investigate what changes in the spectra are caused purely by the tetragonal distortion itself.

When a metal is grown on a substrate, its lattice parameters in different directions will typically be distorted. We have made the following assumptions regarding the lattice parameters of tetragonally distorted Fe, Co, and Ni. For Co and Ni, the in-plane lattice parameter a was set to the experimental Cu bulk value, whereas for Fe, it was set to the experimental bulk lattice parameter of V. Then, the atomic volume was assumed to remain unchanged for all three metals, causing the cubic structure to distort tetragonally. For Fe, this corresponds to a 5.6% expansion of a and a 10.3% decrease of the lattice parameter in the z direction c, relative to the bulk bcc structure. For Co, a is expanded 1.9% and c is decreased by 3.7%, relative to a fcc structure with the same atomic volume as the bulk hcp structure. In the case of Ni, the distortion is roughly on the same level as for Co, with a 2.6% expansion of a and a 5.0% decrease of c, relative to the bulk fcc structure. Obviously, these distortions of Fe, Co, and Ni are highly idealized. In practice the distortion of the lattice may relax continuously as the film thickness is increased. Also, the lattice parameters of the substrate are affected by the metal grown on top of it.

B. Ground-state calculation

In the full-potential linear muffin-tin orbital method (FP-LMTO), which is the density-functional method used in the present study,[41] the Kohn-Sham equations[42] are solved for a general potential without any shape approximation.

For the density functional, we used the local (spin) density approximation (LDA) in the Hedin-Lundqvist parametrization.[43] In the present method, space is divided into nonoverlapping spheres, so-called muffin-tin spheres,[44] surrounding each atomic site, and an interstitial region. The basis functions used are energy independent Bloch functions, whose construction is somewhat different in the spheres and in the interstitial.

A basis function in the interstitial is defined by the Bloch sum of solutions to the spherical Helmholtz equation with nonzero kinetic energy κ^2, or a linear combination of such solutions for different kinetic energies. The Fourier representation of this basis function is taken from the Fourier series of a function matching the basis in the interstitial region but not inside the spheres, a so-called pseudowave function, whose exact shape inside the muffin-tin sphere is of no importance for the final solution as long as it is continuous and differentiable at the sphere boundary and matches the true basis function in the interstitial.

Inside the spheres, where the charge density varies rapidly, the basis functions are Bloch functions of numerical

radial functions times spherical harmonics. The radial part of a basis function is constructed from the numerical solutions $\phi_L(E_\nu,r)$ of the radial Schrödinger equation in a spherical potential at the fixed energy E_ν and their energy derivatives $\dot{\phi}_L(E_\nu,r)$. Here, the index L stands for a collection of quantum numbers: the principal quantum number n, the orbital quantum number l, the magnetic quantum number m, and the kinetic energy κ^2.

The treatment of the entire basis set within one single energy panel allows all states, including the pseudocore states, to hybridize fully with each other. Our method is linear, i.e., the basis functions are constructed by expanding around fixed energies E_ν. The expressions for the crystal wave functions in the muffin-tin spheres are matched to the interstitial crystal wave function at the sphere boundaries so that the total crystal wave function becomes continuous and differentiable in all space. In the present calculation, the expansion in spherical harmonics is taken up to $l=6$, and the $4s$, $4p$, $3d$, and $4f$ orbitals were included in the basis set. For the early $3d$ transition elements, it is important to include the $3p$ semicore states in order to get a converged ground state. For the late transition metals, however, these states can be omitted in a ground-state calculation. Since optical calculations in general require a larger basis set than a ground-state calculation, one could speculate that the $3p$ states could give a significant contribution to the magneto-optical properties, even for the late $3d$ transition elements. However, the pseudocore $3p$ states lie in this case as far as around 4 Ry below the Fermi level, and do not, according to our calculations, affect the magneto-optical spectra. In the ground-state calculation, reciprocal space was sampled with 657 **k** points in the irreducible part of Brillouin zone (IBZ), using special **k**-point sampling methods.[45]

C. Optical calculation

We adopted the dipole approximation in our optical calculations, i.e., the momentum transfer from the initial state to the final state was neglected. Spin-flip transitions, which are allowed within the electric dipole approximation when spin-orbit coupling is included, were also omitted. Guo and Ebert[34] have shown that this simplification changes the optical conductivities by very small amounts, and that it is indeed negligible. With these approximations, the Kubo formula[32] for the absorptive part of the optical conductivity reduces to (with $\alpha\beta=x,y,z$)

$$\sigma_{\alpha\beta}^{(\mathrm{abs})}(\omega)=\frac{Ve^2}{8\pi^2\hbar m^2\omega}\sum_{nn'}\int d^3k\langle \mathbf{k}n|p_\alpha|\mathbf{k}n'\rangle \times\langle \mathbf{k}n'|p_\beta|\mathbf{k}n\rangle f_{\mathbf{k}n}(1-f_{\mathbf{k}n'})\,\delta(\epsilon_{\mathbf{k}n'}-\epsilon_{\mathbf{k}n}-\hbar\omega), \tag{5}$$

in the limit of sharp band states. Note that $\sigma_{\alpha\alpha}^{(\mathrm{abs})}(\omega)=\sigma_{\alpha\alpha}^{(1)}(\omega)$, whereas $\sigma_{\alpha\beta}^{(\mathrm{abs})}(\omega)=\sigma_{\alpha\beta}^{(2)}(\omega)$ when $\alpha\neq\beta$. For a derivation of Eq. (5), see, e.g., Ref. 33. In the above expression, e is the electron charge, m the electron mass, ω the frequency of the incoming/outgoing electromagnetic radiation, $(p_x,p_y,p_z)=\mathbf{p}=-i\hbar\nabla$ the momentum operator, and $|\mathbf{k}n\rangle$ the crystal wave function, corresponding to eigenvalue $E_{\mathbf{k}n}$ with crystal momentum $\mathbf{k}$. $V/8\pi^3$ is the normalization constant of the integral over reciprocal space. Furthermore, $f_{\mathbf{k}n}$ is the Fermi distribution function ensuring that only transitions from occupied to unoccupied states are counted, and $\delta(E_{\mathbf{k}n'}-E_{\mathbf{k}n}-\hbar\omega)$ is the condition for total energy conservation.

The evaluation of the momentum matrix elements in the above equation involves integration in real space. This integration is performed over the muffin-tin spheres and the interstitial separately. Inside the muffin-tin spheres, spherical coordinates are used for the integration. The integral can then be expressed as a radial function times the angular integral. Integration over the angular coordinates in real space, assuming the electric dipole approximation, gives rise to the electric dipole selection rules, i.e., that some of the angular integrals are exactly zero. The nonzero angular integrals can be expressed exactly using Gaunt coefficients and spherical harmonics. The radial integral is, of course, intrinsically numerical, and is evaluated by first performing the differentiation numerically, then integrating. The integral in the interstitial can be rewritten as a surface integral over the muffin-tin spheres using Green's formula. Explicit expressions regarding these integrations can be found in Refs. 46–48.

The integral in reciprocal space is calculated using linear interpolation on a mesh of uniformly distributed points, i.e., the tetrahedron method. Since all information in the problem is contained within the IBZ, the region of integration is the IBZ, giving $\sigma_{ij}^{\mathrm{abs}}(\omega,\mathrm{IBZ})$. The total absorptive part of the optical conductivity $\sigma_{ij}^{\mathrm{abs}}(\omega)$ is then obtained by performing all symmetry operations on $\sigma_{ij}^{\mathrm{abs}}(\omega,\mathrm{IBZ})$, summing up and normalizing with the number of symmetry operations. For the optical calculations, many more **k** points are needed in order to obtain convergence than in the ground-state calculation. We used 11 661 **k** points in the IBZ.

With all absorptive optical conductivities calculated, broadening and Kramers-Kronig transformation still remain. The most common way to broaden is actually to use a constant width, but since the lifetime of an excited state generally decreases with increased excitation energy, it is relevant and potentially more appropriate to broaden with a function whose width increases, in some way, with the excitation energy. Gasche *et al.*[35] let their broadening width increase quadratically with the excitation energy. We have tried this, but found it to work less satisfactorily than the linear prescription. A quadratic broadening removes too much structure at higher energies, where structure definitely still exists in the experimental spectra. Alternatively it gives, compared to experiment, an exaggerated sharpness to the peaks at low energy. This sharpness may of course be removed by convoluting the final spectrum with a Gaussian, but the width required to get reasonable smoothness is too large to correspond to experimental resolution or temperature broadening. Although it is tempting to make use of more elaborate broadening schemes than those discussed here, we have refrained from doing so, since such schemes inevitably imply an increased number of degrees of freedom in the calculation. More advanced schemes would very probably improve the agreement with experiment but at the same time reduce the significance of the result. Thus, broadening the calculated optical spectra was performed by convoluting the absorptive optical conductivity with a Lorentzian whose width was taken to increase linearly with the photon energy.

The corresponding dispersive optical conductivity was then calculated by performing the Kramers-Kronig transformation of the broadened absorptive part. The convergence of the Kramers-Kronig transformation was checked by performing double Kramers-Kronig transformations and comparing the result with the original spectrum. It is our experience that both resolution broadening and thermal broadening can be neglected compared to the lifetime broadening, which dominates completely.

With all parts of the optical conductivity calculated, the polar MOKE spectra are easily evaluated using Eq. (4).

Since several of the previous calculations of the Kerr spectra have been performed using a minimal basis set, we checked what differences using only one κ value would do to our spectra. The resulting Kerr spectra were similar to the ones shown below.

D. Intraband contribution

It is nowadays rather established that at low temperature, direct interband transitions dominate the absorption. The indirect interband transitions can be neglected, or partly accounted for by broadening the spectra suitably. At low energies, below ~ 0.5 eV, intraband transitions, which are always indirect, become important. The intraband contribution for the diagonal components of the conductivity tensor is normally taken into account by means of the Drude formula,

$$\sigma_D(\omega) = \frac{\omega_p^2}{4\pi(\gamma_D - i\omega)}, \tag{6}$$

where ω_p is the unscreened plasma frequency and γ_D the inverse relaxation time of the indirect intraband transitions. The second parameter in the Drude formula, γ_D, is dependent on the amount of vacancies and other defects, and will therefore vary from sample to sample.

We have used the following Drude parameters. Fe: $\gamma_D = 0.45$ eV, $\omega_p = 4.9$ eV; Co: $\gamma_D = 0.5$ eV, $\omega_p = 8.3$ eV; Ni: $\gamma_D = 0.56$ eV, $\omega_p = 7.5$ eV, all taken from Ref. 49. It is worth noting that the extraction of the Drude parameters from experimental data requires a free-electron-like region in the optical spectra.[50] Such a region exists for metals such as aluminum or silver, but not for Fe, Co, or Ni. Experimental determination of the Drude parameters for these metals is therefore intrinsically difficult.

Just as for the diagonal part of the conductivity, the off-diagonal part has a contribution from indirect intraband transitions.[51,52] It is, however, much smaller than in the diagonal case, and although it has been speculated[34] that this contribution could give rise to visible differences in the spectra, we omit this contribution in the present calculation.

IV. RESULTS

Figure 1 shows the experimental and calculated diagonal xx component of the absorptive optical conductivity $\sigma_{xx}^{(1)}$ for cubic and tetragonal Fe, Co, and Ni.

Starting with Fe, we see that the experimental spectra all show the same general trends, but have different amplitudes. The experimental spectra for Fe peak between 2 eV and 3 eV. In the low-energy range, the Drude tail is clearly visible. Our calculated spectrum for the cubic system (solid line) must be said to be in very good agreement with both experimental data and the spectrum calculated by Oppeneer *et al.*,[30] which is also shown in the figure. Note that the Drude contribution is not included in the spectrum calculated by Oppeneer *et al.*

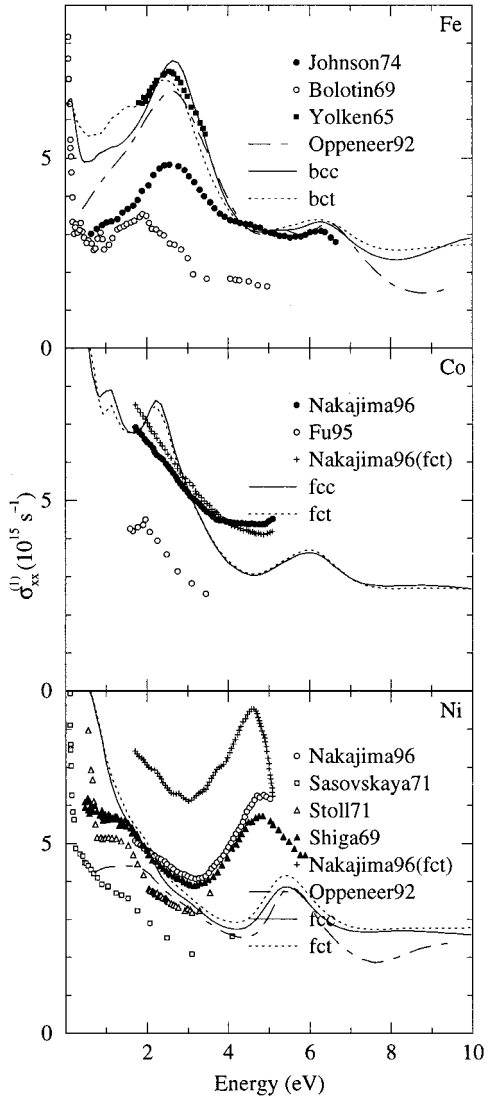

FIG. 1. Calculated diagonal absorptive optical conductivity for cubic (solid lines) and tetragonal (dashed lines) Fe, Co, and Ni. The dot-dashed lines are calculated spectra from Ref. 30. The experimental data shown are as follows. **Fe**: filled circles, Ref. 21; white circles, Ref. 23; and filled squares, Ref. 24. **Co**: filled circles, Ref. 13 (1000 Å film); white circles, Ref. 25; and pluses, Ref. 13 (20 Å film). **Ni**: filled circles, Ref. 13 (1000 Å film); white squares, Ref. 53; filled triangles, Ref. 54; white triangles, Ref. 22; and pluses, Ref. 13 (20 Å film).

The experimental data for cubic Co are less conclusive than in the case of Fe. In the data of Ref. 25, signs of a peak around 2 eV may be traced, and from 2 eV to 6 eV, all experiments exhibit a negative slope. Both these features are reproduced in our calculated spectrum, possibly with the peak displaced slightly toward higher energies.

For Ni, the experimental curves all follow the same trend,

although the absolute amplitudes differ from one experiment to another, just as for Fe. At low energies, the spectrum is dominated by the Drude contribution, giving the tail at energies below 0.5 eV. This tail is followed by a small structure around 1.5 eV, which is reproduced in our calculations, and a broad peak centered around 5 eV, which is also present in the calculated spectra, but shifted to higher energy. Also here, our calculated $\sigma_{xx}^{(1)}$ spectrum for the cubic system is very similar to earlier published calculated spectra,[30,36] both regarding the total amplitude and the peak positions.

For both Fe and Ni, our spectra are flatter at higher energies than other calculated spectra. This is due to our broadening prescription, in which the broadening width increases with the photon energy.

As seen from Fig. 1, the tetragonal distortion affects only marginally the diagonal absorptive optical conductivity. The differences are largest for Fe, which is natural since the tetragonal distortion in the calculations is largest for this element. The main changes are that the maximum peak amplitude is decreased, and that the minimum just after the Drude tail is less pronounced. In the case of Co, the peak at 1.2 eV has become smaller, and for Ni, whose spectrum lacks finer structures in the low-energy region, the changes are minor. For both Co and Ni, experimental spectra derived from measurements on 20 Å thick films grown on Cu are shown (pluses), as well as measurements on 1000 Å thick films (filled circles). In the Co case, the two spectra are rather similar, but for Ni, the amplitude of the spectrum from the 20 Å film is significantly higher than the spectrum for the thicker film. Our results indicate that these spectral changes are not due to tetragonal distortion itself.

In Fig. 2, the calculated off-diagonal absorptive optical conductivity $\sigma_{xy}^{(2)}$ for cubic and tetragonal Fe, Co, and Ni is compared with spectra derived from experimental measurements; see Refs. 13,16,17, and 55–57. The conductivity multiplied by the frequency is plotted, not the conductivity itself. Discrepancies at higher energies are therefore enhanced and appear larger than they are. The tetragonal distortion is seen to result in some changes of the spectra for all three metals, and the change is somewhat larger in this component than in the diagonal conductivity. The off-diagonal conductivity is thus seen to be a more sensitive probe of small changes in the crystal structure.

For Fe, two of the experimental spectra peak around 2 eV and fall off to a shoulder with an almost constant amplitude from 4 eV to 6 eV. The third experimental spectrum is misplaced by about 1 eV in comparison to the two others. Our calculated off-diagonal optical conductivity has a significantly larger amplitude than the experimental spectra. It peaks at 2.2 eV, in close accordance with experiment, and falls off to a shoulder, also in agreement with experiment. It may be noted from Fig. 2 that the sensitivity to structural effects may be quite large, and for certain frequencies the structural distortion modifies the signal with up to $\sim 30\%$.

To our knowledge, there exists only one published experimental measurement of the off-diagonal absorptive optical conductivity for cubic Co, and no calculated spectrum. The experimental spectrum, shown with black circles in the middle panel of Fig. 2, suggests a peak below 2 eV, and exhibits a clear shoulder between 3 eV and 5 eV. Just as for the diagonal absorptive optical conductivity, the Co spectrum is rather similar to that of Fe, with the structures displaced to lower energies for Co. The calculated spectrum exhibits a peak at 2.2 eV and a shoulder at higher energies, which appears to follow the experimental spectrum rather closely.

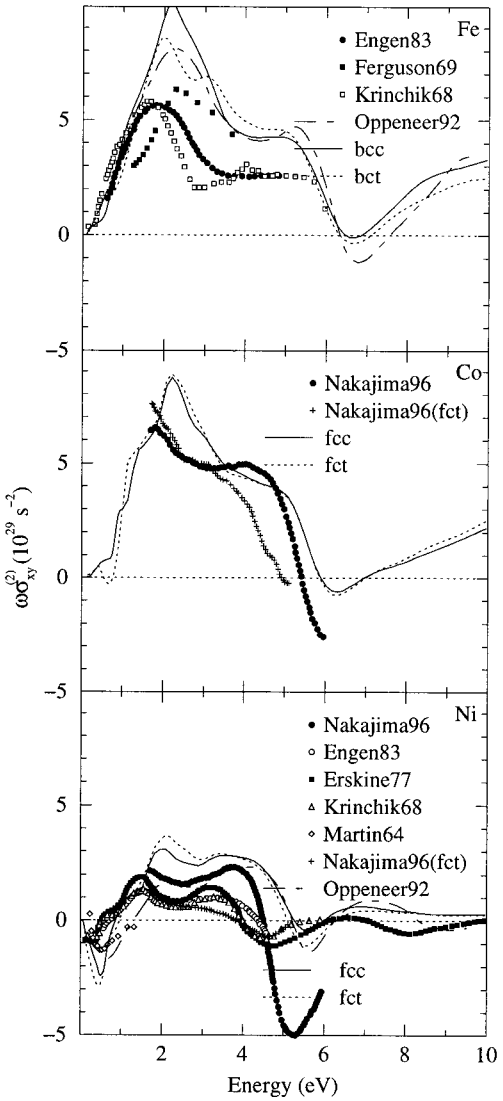

FIG. 2. Calculated off-diagonal absorptive optical conductivity for cubic (solid lines) and tetragonal (dashed lines) Fe, Co, and Ni. The dot-dashed lines are calculated spectra from Ref. 30. The experimental data shown are as follows. **Fe**: filled circles, Ref. 55; filled squares, Ref. 56; white squares, Ref. 17. **Co**: filled circles, Ref. 13 (1000 Å film); pluses, Ref. 13 (20 Å film); **Ni**: filled circles, Ref. 13 (1000 Å film); white circles, Ref. 55; filled squares, Ref. 16; white triangles, Ref. 17; white diamonds, Ref. 57; and pluses, Ref. 13 (20 Å film).

For Ni, our calculated spectrum exhibits the minimum at low energy seen in the experimental spectra, as well as the double-peak structure at intermediate energies. However, all structures appear at higher energies than in the experimental spectra. The total amplitude of the calculated spectrum is higher than that of the experimental spectra, just as in the case of Fe and Co.

For Fe and Ni, spectra calculated by Oppeneer *et al.*[30] are

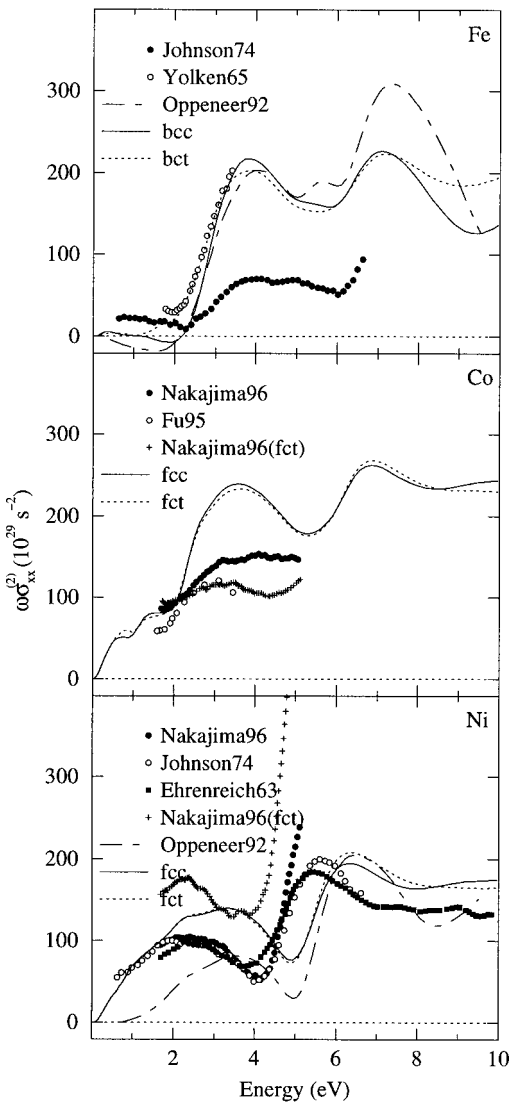

FIG. 3. Calculated diagonal dispersive optical conductivity for cubic (solid lines) and tetragonal (dashed lines) Fe, Co, and Ni. The dot-dashed lines are calculated spectra from Ref. 30. The experimental data shown are as follows. **Fe**: filled circles, Ref. 21; white circles, Ref. 24. **Co**: filled circles, Ref. 13 (1000 Å film); white circles, Ref. 25; and pluses, Ref. 13 (20 Å film). **Ni**: filled circles, Ref. 13 (1000 Å film), white circles, Ref. 21; filled squares, Ref. 26; and pluses, Ref. 13 (20 Å film).

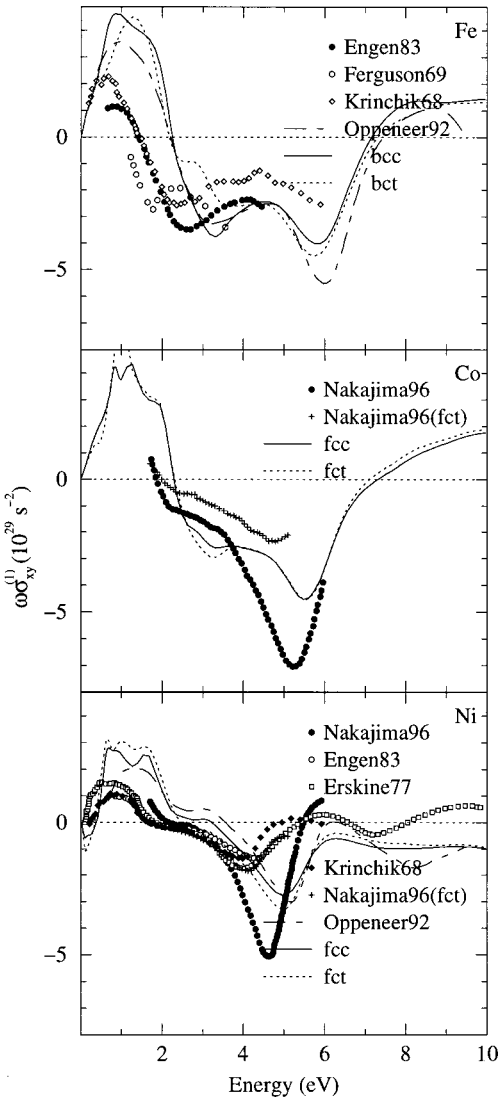

FIG. 4. Calculated off-diagonal dispersive optical conductivity for cubic (solid lines) and tetragonal (dashed lines) Fe, Co, and Ni. The dot-dashed lines are calculated spectra from Ref. 30. The experimental data shown are as follows. **Fe**: filled circles, Ref. 55; white circles, Ref. 56; and white diamonds, Ref. 17. **Co**: filled circles, Ref. 13 (1000 Å film); pluses, Ref. 13 (20 Å film). **Ni**: filled circles, Ref. 13 (1000 Å film); white circles, Ref. 55; white squares, Ref. 16; filled diamonds, Ref. 17; and pluses, Ref. 13 (20 Å film).

also shown. As seen, our spectra are similar to these spectra. However, due to the differences in basis set, there are differences, especially at higher energies, which may signal linearization errors in the minimal basis-set calculations.

We now move on to the dispersive components of the optical conductivity tensor. The diagonal component $\sigma_{xx}^{(2)}$, multiplied by the frequency, is shown in Fig. 3. Just as for the absorptive correspondent, the tetragonal distortion is seen to have only a minor effect on the spectra.

The main reason why the amplitudes in the other calculated spectra[30,36] are lower than our amplitude in the low-energy region is because they have chosen to plot the conductivities without the Drude contribution taken into account. The general effect of this contribution amounts to a positive shift of the amplitude of the dispersive component over the entire energy range. At higher energies, our broadening prescription takes over, producing a flatter curve than the other calculated spectra.

The last conductivity term, i.e., the off-diagonal dispersive optical conductivity $\sigma_{xy}^{(1)}$ multiplied with the frequency, is shown in Fig. 4.

For all three metals, the calculated spectra, both ours and the ones from Ref. 30, have a larger amplitude than the experimental ones at low energies, and the peak positions are shifted toward higher energies. The effect of tetragonal distortion for this component is seen to be largest at the low-frequency part of the spectra. Again it may be found that

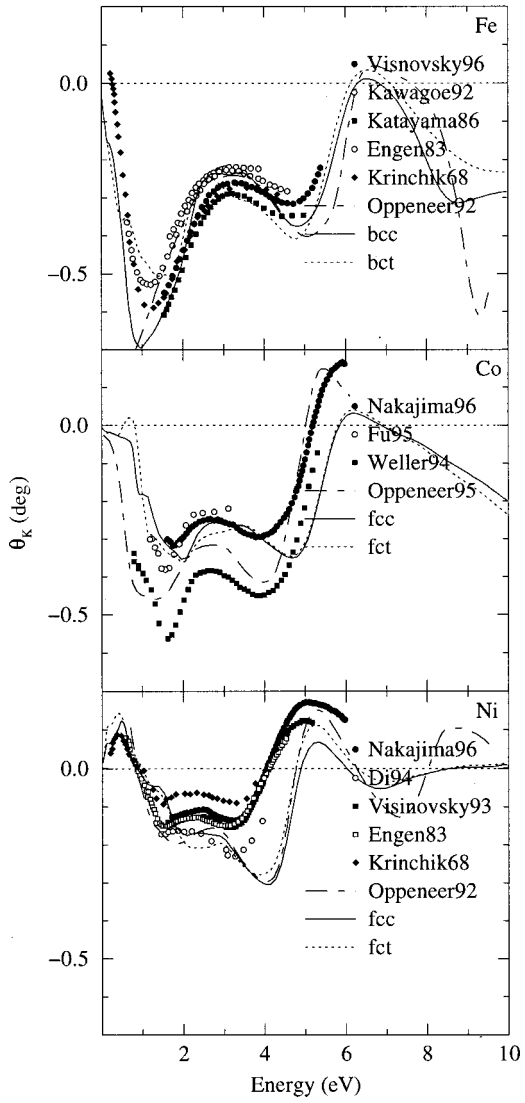

FIG. 5. Calculated polar MOKE rotation for cubic (solid lines) and tetragonal (dashed lines) Fe, Co, and Ni. The dot-dashed lines are calculated spectra from Refs. 30 and 31. The experimental data shown are as follows. **Fe**: filled circles, Ref. 18; white circles, Ref. 58; filled squares, Ref. 59; white squares, Ref. 55; and filled diamonds, Ref. 17. **Co**: filled circles, Ref. 13 (1000 Å film); white circles, Ref. 25; and filled squares, Ref. 19. **Ni**: filled circles, Ref. 13 (1000 Å film); white circles, Ref. 20; filled triangles, Ref. 60; white squares, Ref. 55; and filled diamonds, Ref. 17.

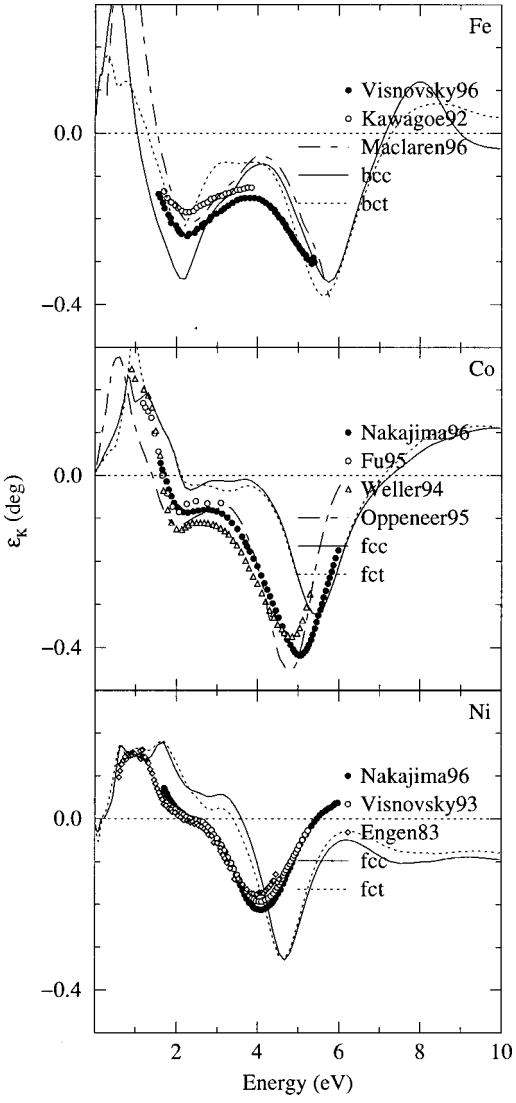

FIG. 6. Calculated polar MOKE ellipticity for cubic (solid lines) and tetragonal (dashed lines) Fe, Co, and Ni. The dot-dashed lines are calculated spectra from Refs. 37 and 31. The experimental data shown are as follows. **Fe**: filled circles, Ref. 18; white circles, Ref. 58. **Co**: filled circles, Ref. 13 (1000 Å film); white circles, Ref. 25; and white triangles, Ref. 19. **Ni**: filled circles, Ref. 13 (1000 Å film); white circles, Ref. 60; and white diamonds, Ref. 55.

methods using different basis sets give somewhat different spectra.

In Fig. 5 experimental (Refs. 13,17–20,25 and 58–60) and theoretical spectra for the polar Kerr rotation are plotted.

In general, the agreement with both experimental spectra and with other calculated spectra is very good. For Co, our calculation follows more closely the experimental spectra in Refs. 13 and 25, whereas the spectrum calculated by Oppeneer *et al.*[31] is in closer agreement with the spectrum of Ref. 19 regarding the peak amplitudes. It is also shifted in energy compared to our spectrum, and the reason is that we have used the experimental lattice parameter, whereas in Ref. 31, an expanded lattice parameter was used in order to correct for the overestimation of the $3d$-band width present in density-functional calculations. Also for Ni, this displacement of the peak positions in the calculated spectra compared to the experimental ones is clearly visible.

The spectrum measured by Di *et al.*[20] for Ni is a low-temperature spectrum. The second minimum in this spectrum is considerably deeper than in the other experimental spectra, indicating that the Kerr rotation spectrum for Ni is rather temperature sensitive. The form of this spectrum, with its deeper second minimum, is in better agreement with the form of our and other calculated Kerr rotation spectra for Ni than the room-temperature spectra.

The tetragonal distortion is seen to change the amplitude of the spectra. For Fe and Ni, the general form remains approximately the same, whereas in the low-energy region of Co, a small positive peak, not present in the cubic spectrum, appears at 0.8 eV for the tetragonally distorted metal.

The polar Kerr ellipticity is shown in Fig. 6. It is interesting to note that the spread in the experimental results is unusually small for this entity; for Ni, the three experimental spectra are practically on top of each other.

The calculated and experimental spectra are generally in very good agreement. For Co, again, our spectrum is displaced toward higher energies compared to the spectrum calculated by Oppeneer *et al.*,[31] because of the lattice-parameter effect.

Just as for the Kerr rotation, the effect of tetragonal distortion is clearly visible, especially in the low-energy part of the spectra. For Fe, the positive low-energy peak decreases significantly, and so does the amplitude of the shoulder at 2 eV. In contrast, the amplitude of the low-energy peak in Co increases. This is also the case for Ni, although here the effect is not as pronounced.

V. DISCUSSION AND CONCLUSIONS

In conclusion, the tetragonal distortion has a clearly visible effect on the calculated off-diagonal conductivities, and therefore on the MOKE signal. However, the effect is far from as large as indicated in Ref. 13. This implies that the differences seen between 1000 Å and 20 Å films most probably have other origins. In Ref. 13, lattice mismatch at the interface, increased atomic volume, and reduced atomic coordination number in the surface and interface are mentioned. To this list one might add island formation and surface and interface roughness. Another possible explanation of these differences is that in Ref. 13, the conductivities for the 20 Å film have been calculated from longitudinal Kerr measurements, whereas the conductivities for the 1000 Å film were derived from measured polar Kerr spectra. The longitudinal Kerr effect is a much smaller effect than the polar Kerr effect, and uncertainties of measurement should therefore affect the longitudinal signal to a larger extent. This might explain the large differences in amplitude of the conductivities.

In this paper, only changes in the interband contribution have been considered so far. The Fermi surface of course changes due to the tetragonal distortion, and therefore the plasma frequency should also change. Furthermore, the relaxation frequency in a thin film is expected to be different from the bulk value. Thus, it is reasonable to assume that Drude parameters change in the thin film as compared to the bulk. Changes in these parameters indeed affect the positions and amplitudes of the main peaks of the Kerr signal. However, the experimentally observed changes in the off-diagonal conductivities can hardly be explained this way, since they are virtually independent of the Drude contribution.

Experimentally, the amplitude of the Kerr signal is often taken as a direct measure of the magnetic moment. An important result of our calculations is that the calculated spin moment in fact changes very little as a function of the tetragonal distortion. The relative change of the orbital moment is much larger, but since this moment is very small compared to the spin moment, this gives a negligible effect on the total moment.[61] Thus, the distortion-induced changes in the magneto-optical spectra are not due to a change in the spin polarization of the material, and no simple relation exists between the magnitude of the polar MOKE signal and the spin moment, if at the same time the material's crystal structure is being changed, e.g., being tetragonally distorted. As a film grows, the tetragonal distortion normally does change, and thus using the MOKE signal as a measure of the spin moment can be misleading in such cases.

In a general comparison of calculated magneto-optical spectra of Fe, Co, and Ni, using different calculational approaches, it is safe to say that all methods give rather similar results for these close-packed systems. The main differences between different calculations seem to be in the absolute amplitude of the conductivities. Our calculations show larger total amplitudes, both of the diagonal and off-diagonal absorptive optical conductivities, than the spectra calculated by Oppeneer *et al.*[30] and by Mainkar *et al.*[36] For more open crystal structures, we expect the full-potential treatment to be of more importance. Also, at higher energies it seems like the minimal basis-set methods deviate somewhat from the multibasis method presented here, which may be due to linearization errors.

A general difference between calculated and experimental absorptive conductivities appears to be that the amplitudes are systematically larger in the calculations. This is quite expected, since there is always an unavoidable loss in a measurement. Also, in all published calculated spectra of the optical conductivities as well as the polar Kerr signal, the peaks are displaced toward higher energies with respect to experimental spectra. This tendency is smallest for Fe and largest for Ni. From the density-functional calculations made on these systems, it has become quite clear that especially for Ni, an essential part in the electronic structure is missing in the density-functional description. For example, DFT overestimates the $3d$-band width in these metals, which in turn affects the optical and magneto-optical spectra and causes peaks to be offset toward higher energies. By increasing the lattice parameter, this discrepancy can be artificially corrected, since a larger lattice parameter gives narrower bands.[30] A most interesting development, and a more physically appealing way of correcting for the overestimated $3d$-band width, would be to perform GW-corrected calculations[62] of the magneto-optical spectra. Such an approach has been shown to give a band structure for Ni in closer agreement with experiment.[63]

ACKNOWLEDGMENTS

Valuable discussions with P. M. Oppeneer, T. Kraft, J. Hunter-Dunn, and P. Isberg are acknowledged. M. Alouani and R. Ahuja are acknowledged for taking part in the implementation of the electric dipole matrix elements in the FP-LMTO program. This work was financed by the Swedish Research Council for Engineering Sciences and the Swedish Natural Science Foundation. We also acknowledge the Psik-network.

[1] R. Pittini *et al.*, Phys. Rev. Lett. **77**, 944 (1996).
[2] J. Reif, J. C. Zink, C.-M. Schneider, and J. Kirschner, Phys. Rev. Lett. **67**, 2878 (1991).
[3] H. R. Hulme, Proc. R. Soc. London, Ser. A **135**, 237 (1932).
[4] C. Liu, E. R. Moog, and S. D. Bader, Phys. Rev. Lett. **60**, 2422 (1988); C. Liu and S. D. Bader, J. Magn. Magn. Mater. **93**, 307 (1991).
[5] W. R. Bennett, W. Schwarzacher, and W. F. Egelhoff, Phys. Rev. Lett. **65**, 4971 (1989).
[6] W. B. Zeper, F. J. A. M. Greidanus, P. F. Garcia, and C. R. Fincher, J. Appl. Phys. **65**, 4971 (1989); D. Weller, H. Brändle, G. Gorman, C.-J. Lin, and H. Notarys, Appl. Phys. Lett. **61**, 2726 (1992).
[7] See, e.g., M. H. Kryder, J. Appl. Phys. **57**, 3915 (1985).
[8] J. Schoenes, in *Materials Science and Technology*, edited by K. H. J. Buschow (VHC, New York, 1992), Vol. 3A, p. 147.
[9] H. Ebert, Rep. Prog. Phys. **59**, 1665 (1996).
[10] P. M. Oppeneer, V. N. Antonov, A. N. Yaresko, A. Ya. Perlov, T. Kraft, and H. Eschrig, J. Magn. Soc. Jpn. **20**, 41 (1996).
[11] P. M. Oppeneer and V. N. Antonov, in the *Proceedings of Spin-orbit-influenced Spectroscopies of Magnetic Solids* (Springer, Berlin, 1996), p. 29.
[12] K. H. J. Buschow, in *Ferromagnetic Materials*, edited by E. P. Wohlfarth and K. H. J. Buschow (North-Holland, Amsterdam, 1988), Vol. 4, Chap. 5.
[13] K. Nakajima, H. Sawada, T. Katayama, and T. Miyazaki, Phys. Rev. B **54**, 15 950 (1996).
[14] T. Suzuki, D. Weller, C. A. Chang, R. Savoy, T. Huang, B. A. Gurney, and V. Speriosu, Appl. Phys. Lett. **64**, 2736 (1994).
[15] J. L. Erskine and E. A. Stern, Phys. Rev. Lett. **30**, 1329 (1973).
[16] J. L. Erskine, Physica B & C **89B**, 83 (1977).
[17] G. S. Krinchik and V. A. Artemjev, Zh. Éksp. Teor. Fiz. **53**, 1901 (1967) [Sov. Phys. JETP **26**, 1080 (1968)]; J. Appl. Phys. **39**, 1276 (1968).
[18] Š. Višňovský, R. Krishnan, M. Nýlt, and P. Prosser (unpublished).
[19] D. Weller, G. R. Harp, R. F. C. Farrow, A. Cebollada, and J. Sticht, Phys. Rev. Lett. **72**, 2097 (1994).
[20] G. Q. Di and S. Uchiyama, J. Appl. Phys. **75**, 4270 (1994).
[21] P. B. Johnson and R. W. Christy, Phys. Rev. B **9**, 5056 (1974).
[22] M. Shiga and G. P. Pells, J. Phys. C **2**, 1847 (1969).
[23] G. A. Bolotin, M. M. Kirillova, and V. M. Mayevskiy, Fiz. Met. Metalloved. **27**, 224 (1969).
[24] H. T. Yolken and J. Kruger, J. Opt. Soc. Am. **55**, 842 (1965).
[25] H. Fu, Z. Yan, S. K. Lee, and M. Mansuripur, J. Appl. Phys. **78**, 4076 (1995).
[26] H. Ehrenreich, H. R. Philipp, and D. J. Olechna, Phys. Rev. **131**, 2469 (1963).
[27] H. Ebert, Habilitation thesis, University of Munich, 1990.
[28] B. Cooper *et al.*, IEEE Trans. Magn. **27**, 3648 (1991).
[29] S. V. Halilov and Yu. A. Uspenskii, J. Phys.: Condens. Matter **2**, 6137 (1990).
[30] P. M. Oppeneer, T. Maurer, J. Sticht, and J. Kübler, Phys. Rev. B **45**, 10 924 (1992); Z. Phys. B: Condens. Matter **88**, 309 (1992).
[31] P. M. Oppeneer, T. Kraft, and H. Eschrig, Phys. Rev. B **52**, 3577 (1995).
[32] R. Kubo, J. Phys. Soc. Jpn. **12**, 570 (1957).
[33] C. S. Wang and J. Callaway, Phys. Rev. B **9**, 4897 (1974).
[34] G. Y. Guo and H. Ebert, Phys. Rev. B **50**, R10 377 (1994); **51**, 12 633 (1995).
[35] T. Gasche, M. S. S. Brooks, and B. Johansson, Phys. Rev. B **53**, 296 (1996).
[36] N. Mainkar, D. A. Browne, and J. Callaway, Phys. Rev. B **53**, 3692 (1996).
[37] J. M. Maclaren and W. Huang, J. Appl. Phys. **79**, 6196 (1996).
[38] P. S. Pershan, J. Appl. Phys. **38**, 1482 (1967).
[39] D. H. Martin, K. F. Neal, and T. J. Dean, Proc. Roy. Phys. Soc. London **86**, 605 (1965).
[40] F. J. Kahn, P. S. Pershan, and J. P. Remeika, Phys. Rev. **186**, 891 (1969).
[41] J. M. Wills (unpublished); J. M. Wills and B. R. Cooper, Phys. Rev. B **36**, 3809 (1987); D. L. Price and B. R. Cooper, *ibid.* **39**, 4945 (1989).
[42] P. Hohenberg and W. Kohn, Phys. Rev. **136**, B864 (1964); W. Kohn and L. J. Sham, Phys. Rev. **140**, A1133 (1965).
[43] L. Hedin and B. I. Lundqvist, J. Phys. C **4**, 2064 (1971).
[44] O. K. Andersen, Phys. Rev. B **12**, 3060 (1975); H. L. Skriver, *The LMTO Method* (Springer, Berlin, 1984).
[45] D. J. Chadi and M. L. Cohen, Phys. Rev. B **8**, 5747 (1975); S. Froyen, *ibid.* **39**, 3168 (1989).
[46] M. Alouani and J. M. Wills, Phys. Rev. B **54**, 2480 (1996).
[47] R. Ahuja, S. Auluck, J. M. Wills, M. Alouani, B. Johansson, and O. Eriksson, Phys. Rev. B **55**, 4999 (1997).
[48] T. Gasche, Ph.D. thesis, Uppsala University, 1993.
[49] A. P. Lenham and D. M. Treherne, in *Optical and Electronic Structure of Metals and Alloys*, edited by F. Abelès (North-Holland, Amsterdam, 1966), p. 1966.
[50] C. G. Ribbing (private communication).
[51] J. Erskine and E. Stern, Phys. Rev. B **8**, 1239 (1973).
[52] W. Reim, O. Hüsser, J. Schoenes, E. Kaldis, P. Wachter, and K. Seller, J. Appl. Phys. **55**, 2155 (1984).
[53] I. I. Sasovskaya and M. M. Naskov, Fiz. Met. Metalloved. **32**, 723 (1971); **33**, 86 (1972).
[54] M. Ph. Stoll, Solid State Commun. **8**, 1207 (1971).
[55] P. G. van Engen, Ph.D. thesis, Technical University Delft, 1983.
[56] P. E. Ferguson and R. J. Romagnoli, J. Appl. Phys. **40**, 1236 (1969).
[57] D. H. Martin, S. Doniach, and K. J. Neal, Phys. Lett. **9**, 224 (1964).
[58] T. Kawagoe and T. Mizoguchi, J. Magn. Magn. Mater. **113**, 187 (1992).
[59] T. Katayama, H. Awano, and Y. Nishihara, J. Phys. Soc. Jpn. **55**, 2539 (1986).
[60] S. Visnovsky, V. Parizek, M. Nyvlt, P. Kielar, V. Prosser, and R. Krishnan, J. Magn. Magn. Mater. **127**, 135 (1993).
[61] P. James (private communication).
[62] L. Hedin, Phys. Rev. **139**, A796 (1965); L. Hedin and S. Lundqvist, in *Solid State Physics, Andvances in Research and Application*, edited by F. Seitz, D. Turnbull, and H. Ehrenreich (Academic, New York, 1969), Vol. 23, p. 1.
[63] F. Aryasetiawan, Phys. Rev. B **46**, 13 051 (1992).